Hydrol. Earth Syst. Sci. Discuss., 12, 4191–4231, 2015
www.hydrol-earth-syst-sci-discuss.net/12/4191/2015/
doi:10.5194/hessd-12-4191-2015

Hydrology and Earth System Sciences
Open Access
Discussions

Updating hydraulic properties and layer thicknesses in hydrogeological models using groundwater model calibration results

A. Lourens[1], **M. F. P. Bierkens**[1,2], **and F. C. van Geer**[1,3]

[1]Department of Physical Geography, Faculty of Geosciences, Utrecht University, Heidelberglaan 2, 3584 CS Utrecht, the Netherlands
[2]Unit Subsurface and Groundwater Systems, Deltares, Princetonlaan 6, 3584 CB Utrecht, the Netherlands
[3]TNO Geological Survey of the Netherlands, Princetonlaan 6, 3584 CB Utrecht, the Netherlands

Received: 27 March 2015 – Accepted: 3 April 2015 – Published: 24 April 2015

Correspondence to: A. Lourens (a.lourens@uu.nl)

Published by Copernicus Publications on behalf of the European Geosciences Union.

Abstract

Usually, subsoil data for groundwater models are generated from borehole data, using upscaling techniques. Since the assumed hydraulic properties for litho-classes in boreholes are uncertain, and upscaling may add inaccuracies, the groundwater model has to be calibrated. In this paper, a method is presented that uses a calibrated groundwater model to improve the quality of a hydrogeological model (layer thickness and hydraulic properties) as obtained from borehole data. To achieve this, all borehole data are defined by random variables and related to aquifer and aquitard properties at the same support as the groundwater model, using complete probability density functions. Subsequently, the calibrated parameter values of the groundwater model are assumed to be the truth and are used to find the most likely combination of layer thicknesses and hydraulic conductivities for the lithological layers making up the aquifer or aquitard. The presented example is an application of the proposed method to aquitards. Nevertheless, the method can be applied to aquifers as well. The analysis of the results gives rise to the discussion about the correctness of the hydrogeological interpretation of the borehole data as well as the correctness of the calibration results of the groundwater flow model. In order to make the problem tractable, computationally feasible, and avoid assumptions about the distribution form, piecewise linear probability density functions are used, instead of parametrized functions.

1 Introduction

A clear understanding of the subsoil is important when building hydrogeological and groundwater models. Because the subsoil is generally sparsely observed, only limited information is available about its properties. Building a hydrogeological model of the subsoil is therefore a challenging task with many uncertainties. Identification of deposits with distinct hydraulic properties, at observed and unobserved locations, is vital for the creation of such a model (e.g., Nilsson et al., 2007; Rogiers et al., 2014). Hydrogeolog-

HESSD
12, 4191–4231, 2015

ical models are usually based on borehole descriptions, where the hydraulic properties at the level of litho-layers are described. The thickness of these litho-layers is generally in the order of centimeters to meters. The information from the borehole data has to be interpolated to arrive at spatial fields of hydraulic parameters, such as conductivity or resistance. As a result of the heterogeneity of the subsoil, the effective conductivity of the model grid cells are scale-dependent. The upscaling of the borehole data to model data is therefore a process of major importance and has to be applied carefully. A vast amount of literature is available on this topic (e.g., Dagan, 1986; Nœtinger et al., 2005; Sanchez-Vila et al., 2006; Fiori et al., 2011). In a dynamic groundwater model, the spatially distributed parameter values of the model-layers are adjusted to fit the observed groundwater heads in space as well as in time (e.g., Zimmerman et al., 1998; Valstar et al., 2004; Carrera et al., 2005; Hendricks Franssen et al., 2009; Hoteit et al., 2012). However, these describe the adjustments of the conductivity and resistance of the model-layers. Most calibration procedures do not guarantee adjustments that are plausible (or even feasible) from a geological point of view. In principle, the adjustment of the model-layers properties of the groundwater model holds information on how to adjust the hydraulic properties and thickness of the litho-layers and reduce the associated uncertainty.

The aim of this study is to find the most likely (hydro)geological representations of the subsoil by using results from a calibrated groundwater model. These improvements include the litho-layer thickness and conductivity for each model grid cell.

In this study, a readily calibrated groundwater model, namely the Azure groundwater model (de Lange and Borren, 2014), is used. Although we realize that the calibration might be influenced by misconceptions and sparsely distributed data, and therefore is subject to uncertainty itself, for now we assume that the calibrated aquifer or aquitard properties represent the true parameter values. The subsoil parameterization of the Azure model is mainly derived from the data of the REGIS information system (Vernes et al., 2005; Vernes and van Doorn, 2006). This REGIS system contains interpreted borehole descriptions, and a hydrogeological model. In this hydrogeological model, the

HESSD
12, 4191–4231, 2015

litho-classes, as recognized in the borehole descriptions, are assigned to layers with mainly high conductivity deposits (aquifers) or low conductivity deposits (aquitards). The conductivity of each litho-class is defined by a PDF which is spatially uniform. The PDF of the horizontal and the vertical conductivity are both defined. Beside the borehole information, also knowledge of geological processes is used to define the extent of the hydrogeological layers. The hydrogeological model of REGIS is defined on a scale suitable to the needs of the groundwater modeler. More specific, the support scale of the parameters conductivity and resistance in Azure and REGIS are the same. The connection between the hydrogeological model layers of REGIS and the groundwater model layers of Azure is known. This is an important requirement of the proposed method. On one hand, the litho-class parameters, the layer thickness and conductivity, are described by their respective PDFs. On the other hand, the calibrated groundwater model parameters are assumed to be the truth. The presented method returns the most likely conductivities and thicknesses of the litho-layers, given the prior statistics of the litho-layers and the calibrated dynamic groundwater flow model. Since we assume the calibrated values being the truth, the thickness and properties of the litho-layers exactly match the calibrated values of the model. The support scale of the final results is horizontally equal to the groundwater model scale. Vertically, the results are translated to the litho-layers.

With the proposed method, effects of prior assumptions concerning the litho-layers can be analyzed, and discrepancies between the geological and hydrological interpretation of the subsoil become clear. These discrepancies show up as very unlikely values of the litho-class thickness or conductivities, or unlikely combinations of these parameter values. Herewith, our method not only yields the most likely litho-layer properties, it may also serve as a communication tool between the geologist and the groundwater modeler as well.

This paper is organized as follows. In Sect. 2 the methodology is described, which, in this paper, focuses on the resistance of aquitards. In Sect. 3 the study area and the

HESSD
12, 4191–4231, 2015

data used are presented. The results are presented in Sect. 4. In Sect. 5 the method is discussed and conclusions are drawn.

2 Methodology

2.1 Update algorithm

The proposed method is applicable to the vertical resistance of an aquitard as well as to the transmissivity of an aquifer. In this paper, we focus on the vertical resistance of aquitards.

The vertical resistance of a litho-layer can be derived from observations of the layer thickness and the vertical conductivity of the deposits. These observations always yield uncertain parameter values and they might not be representative for the required model scale. In the REGIS information system (Vernes et al., 2005; Vernes and van Doorn, 2006) these observations are up scaled to be representative for groundwater models such as Azure. The uncertain parameters are treated as random variables described by their probability density functions (PDF). In this paper, all random variables (RV) are described by piecewise linear PDFs (Kaczynski et al., 2012; Vander Wielen and Vander Wielen, 2015) from which all calculations can be performed independent of the type of distribution assumed.

Since the resistance depends on the vertical conductivity and the thickness of the litho-layer, we need the PDF of both. The PDFs of the vertical conductivity are available from earlier studies and, in the Netherlands, supplied by the REGIS information system. The full PDF of the thickness can not be obtained from existing data bases. In practice, often only the mean or mode of the distributions is used to represent the layer thickness. In our method we need the full PDF. In Sect. 2.4 we describe how we obtained the PDFs of the litho-layer thickness.

Let the value of the vertical resistance of an aquitard at grid block u ($c_m(u)$) be the result of the calibration of a groundwater model, in this study obtained from the cali-

HESSD
12, 4191–4231, 2015

brated groundwater model Azure (de Lange and Borren, 2014). This calibrated resistance is assumed to be the best estimate of the vertical resistance of the model-layer given the observation data used for the calibration. In this study, no uncertainty of the calibrated groundwater model is included, so $c_m(u)$ is treated as a deterministic parameter. Furthermore, in accordance with REGIS, we assume that the PDF of the hydraulic conductivity for a given litho-layer does not change in space.

The vertical resistance of a litho-layer is calculated as

$$C_l(u) = D_l(u)/K_l, \tag{1}$$

where C is the vertical hydraulic resistance, D is the layer thickness, K the location independent vertical hydraulic conductivity, l the litho-class, and u denotes the location. The variables C, D, and K are RVs with D and K assumed statistically independent. This independence assumption is reasonable since the study area is relative small with a deposition of sediment under similar geological circumstances. However, a result of the proposed method in a larger study area may give rise to revise this assumption. Subsequently, the total aquitard resistance is defined as a summation of the resistance of all litho-layers as

$$C_{1\ldots n}(u) = \sum_{l=1}^{n} C_l(u), \tag{2}$$

where n is the number of litho-classes in the aquitard. The summation of a subset of l litho-classes can be written as

$$C_{1\ldots l}(u) = C_{1\ldots l-1}(u) + C_l(u). \tag{3}$$

With expressions Eqs. (1) and (2) a $2n$-dimensional joint distribution can be constructed from the n marginal distributions $D_l(u)$ and n marginal distributions K_l. The aim is to find the maximum likelihood (ML) value (Mood et al., 1974, p. 278), conditional to

HESSD
12, 4191–4231, 2015

$c_{1\ldots n}(u) = c_m(u)$. Figure 1 shows the connection of the joint PDF (Fig. 1a) with the probability density function (Fig. 1b), and the maximum likelihood function (MLF) (Fig. 1c). The derivation of the calculations of the MLF, using piecewise linear PDFs, is given in Appendix A. For easy reading of the graphs, the relative probability densities are presented for the joint PDF and the MLF, that is, all depicted densities are proportional to the maximum density of the joint PDF. As an example, the vertical resistance $C = 30\,900$ d is shown. The integration of the densities along the gray line $C = 30\,900$ d is the probability density of the PDF for this C value. The corresponding cumulative probability is calculated through the integration of the densities in the shaded area. The function value for the MLF for the same line is the maximum joint density value found at this line. The dashed black line shows the path of the MLF in the joint PDF. This curve intersects every line of constant C value at its maximum density value. Figure 1c shows the complete MLF. Figure 1a shows only a part of the complete joint PDF, therefore the line of the MLF runs out of sight at the upper edge. The discussed functions are all described piecewise linear, therefore the function values are calculated for a discrete number of C values (gray lines).

Because of this piecewise linearity, no analytical solution is available to find the most likely marginal layer thicknesses ($d_l(u)$) and conductivity values ($k_l(u)$). Since it is hardly possible to find the ML values in such $2n$-dimensional joint PDF simultaneously, a stepwise algorithm is performed using 2-dimensional joint functions at a time. Firstly, for each litho-class l the MLF of the vertical resistance $C_l(u)$ is calculated (Eq. 1), using the PDFs of $D_l(u)$ and K_l as the marginal distributions. Secondly, all vertical resistances are summed step by step (Eq. 3), using the MLFs of the former steps as the marginal distributions. Finally, the most likely marginal values are determined, in the reverse order of former steps, starting with the joint distribution $C_n(u) + C_{1\ldots n-1}(u)$ conditional to $c_{1\ldots n}(u) = c_m(u)$. Where in Eq. (1) K_l is location independent, the most likely value $k_l(u)$ depends on location u since $C_l(u)$ is location dependent.

With this method, a multidimensional joint PDF can successively be evaluated to find the ML values of all marginal distributions.

HESSD
12, 4191–4231, 2015

2.2 Assessment of prior uncertainty per grid cell

The update algorithm, as described in the former section, needs for each litho-class the PDFs of the layer thickness and the conductivity at each grid cell. In the information system REGIS, a PDF of the hydraulic conductivity is assigned to each litho-class, independent of the spatial coordinates. So everywhere in the subsurface where a particular litho-class exists, the probability distribution of the hydraulic conductivity is assumed to be known. Therefore, only the PDFs of the layer thickness for each litho-class have to be spatially predicted. This spatial prediction is performed by using ordinary kriging (OK). For every litho-class in the study area, a semi-variogram model for the litho-layer thickness is estimated. Since layer thicknesses are greater than or equal to zero, the interpolation method must account for this (Tolosana-Delgado and Pawlowsky-Glahn, 2007). In Sect. 4.4, several interpolation options are evaluated to select the most appropriate ones, concerning the observed data.

Using kriging interpolation, the estimation of the interpolated thickness $\hat{D}(u_0)$ at the unobserved location u_0 writes (Isaaks and Srivastava, 1989, p. 282)

$$\hat{D}(u_0) = \sum_{\alpha=1}^{n} \lambda_\alpha D(u_\alpha), \tag{4}$$

where n is the number of observations, λ_α are the kriging weight factors, and $D(u_\alpha)$ are the observations at the locations u_α. Usually, the observations $D(u_\alpha)$ are treated as scalar values. In this study, $D(u_\alpha)$ is the complete PDF of the layer thicknesses, described as a piecewise linear PDF. This method yields a PDF of the interpolated litho-layer thickness $\hat{D}(u_0)$. Subsequently, the PDF of the interpolation ($\hat{D}(u_0)$) and the PDF of the interpolation error are added to achieve a PDF containing all uncertainties. In previous work, this method is described in detail (in preparation for publication). Generation of the PDF of the litho-layer thickness of the observations is described in Sect. 2.4

HESSD
12, 4191–4231, 2015

Ordinary kriging (OK) tends to generate negative weight factors, beside the positive ones, when the spatial distribution of the observations is somehow unbalanced around the estimation location, known as the screen effect. Apart from the physical meaning of negative weight factors, this influences the interpolated result (Goovaerts, 1997, p. 176). To avoid this, the kriging algorithm is modified as described by Deutsch (1996). Herewith, the observation location with the most negative weight factor is removed from the subset of locations for the current kriging location. This is repeated until no negative weight factors are calculated anymore, or until less than the required minimum number of observations is reached. In the latter case, a missing value is assigned to the corresponding kriged location.

Subsequently, the PDF of the vertical hydraulic resistance is obtained by division of the PDF of the interpolated litho-layer thickness by the PDF of the vertical hydraulic conductivity (Eq. 1). The PDFs of the vertical resistance of all litho-classes are added up which yields the PDF of the total vertical hydraulic resistance of the aquitard. For each grid cell these PDFs are subsequently processed with the maximum likelihood algorithm, as described in Sect. 2.1, with the calibrated resistance $c_m(u)$ as parameter.

2.3 Data preparation

The described method needs complete borehole descriptions for a model-layer (aquifer or aquitard) at all borehole locations. Therefore, when a description is incomplete for a borehole, this borehole is neglected for that layer.

Within the extent of the study area and within the considered model-layer, a limited set of litho-classes is found. Because of heterogeneity of the subsurface, not every litho-class is present at every borehole location. However, the absence of a litho-class in a certain borehole is an observation as well. Therefore, when a litho-class is absent in a borehole, it is added with a zero layer thickness. The assignment of the variance to the layer thickness is described in Sect. 2.4.

A litho-class may appear multiple times within one model-layer in one borehole. The thicknesses and variances of all these occurrences are added to one thickness and

HESSD
12, 4191–4231, 2015

variance before further processing. Consequently, the horizontal connectivity of individual litho-layers of a litho-class between boreholes is neglected.

2.4 Layer thickness uncertainty

The method presented in the former sections needs a quantification of the uncertainty of litho-layer thicknesses. However, no quantitative data about this uncertainty are available. In this section, a method is described to provide all litho-layers of the borehole descriptions with an appropriate uncertainty.

During drilling of a borehole, the measured layer thicknesses are always rounded off. This causes uncertainty in the layer thickness. The magnitude of the round-off error depends, for instance, on the drilling method and the way the borehole descriptions are made. Therefore, it is likely that drilling methods which can distinguish the layers more accurately have a smaller round-off error than drilling methods with a lower accuracy. Reversing this reasoning it may be concluded that small round-off values give a more accurate layer thickness than large round-off values. The question is how to recognize the order of magnitude of round-off error in the borehole description data.

From the REGIS data base, about 475 000 litho-layer thicknesses of about 16 000 borehole descriptions are available. The remainder of all these thicknesses, when dividing by one meter, is calculated and shown as a cumulative distribution in Fig. 2. From this figure, it can be seen that round off to one meter (remainder is 0) is done very often (44 %). Also round off to fifty (12 %), ten (30 %) and five (8 %) centimeters is done more often than to one (6 %) centimeter. Truncation to a smaller value than one centimeter is not stored in the data base. The number of layers in each truncation class is counted after removing the layers counted in a higher truncation class (a class with a higher round-off value). Obviously, values of layers of a lower class often coincide with values of a higher class. This makes the above counting biased. Although this can be statistically corrected for the distribution as a whole, it can not easily be corrected for the individual layers. Therefore, no correction is applied and this error is accepted in the described method.

HESSD
12, 4191–4231, 2015

Since no quantitative information is available about the uncertainty of the litho-layer thicknesses, an arbitrary choice has to be made. To justify the choice, a sensitivity analysis is carried out to test the performance of different options. These options include two types of distributions, and the magnitude of the variance. When the type of distribution is unknown, the normal distribution is usually a safe choice, because the round-off errors may be assumed symmetric around zero. Since the normal distribution may yield negative layer thicknesses, the log-normal distribution is tested as well. The standard deviation for each litho-layer is linearly related to its truncation class value using a fixed factor for each standard deviation class (Table 1). For the low standard deviation class this factor is 1/5, for the medium class 1, and for the high class 5.

When a litho-class is observed absent in a borehole, it should get a thickness of 0 m. However, an expected thickness value of zero yields problems with the assignment of a PDF to this observation. When a normal distribution is chosen, the layer thickness will be less then zero with a probability of 0.5. With the choice of a log-normal distribution it is impossible to assign a variance greater than zero to the observation. Therefore, a small positive value has to be chosen for the 0-thickness observations. The choice of an appropriate value is described in Sect. 4.3.

3 Study area and available data

The location of the study area is shown in Fig. 3. The size of this area is 20 km × 25 km with a grid size of 100 m × 100 m. The used borehole data originate from borehole descriptions as administered by the Geological Survey of the Netherlands and the hydrogeological interpretations as stored in the REGIS information system. In REGIS, litho-classes are assigned to all identified layers from every borehole. The definition of the litho-classes is based on lithological properties and lithostratigraphical units. Each litho-class is provided with two probability density functions (PDF) of the hydraulic conductivity, one for the horizontal conductivity and one for the vertical conductivity. Subsequently, these litho-classes are aggregated to hydrogeological units, namely aquifers

HESSD
12, 4191–4231, 2015

and aquitards. These data are thus suitable to be used in numerical groundwater models. The data include layer depths, litho-classes, and hydrogeological units.

The calibrated layer properties (transmissivity and resistance values) originate from the Azure groundwater model, developed by Deltares, the Netherlands (de Lange and Borren, 2014). This groundwater model is based on the hydrogeological model from REGIS and therefore suitable to perform this study.

In this paper, we focus on the fourth aquitard in the Azure groundwater model. This aquitard is a high vertical resistance clay patch, surrounded by an area where the clay layer is thin or absent. This aquitard is found between 20 and 85 m below surface level. To meet the numerical requirements of the groundwater model, a minimum vertical resistance of one day is used in the area where the aquitard is absent. The calibrated vertical resistance of the aquitard and the ratio calibrated/uncalibrated resistance are depicted in Fig. 4.

The aquitard consists of seven different litho-classes. The hydraulic properties of these litho-classes, as defined in REGIS, are shown in Table 2. Not all litho-classes do have characteristic properties for aquitards. The sand classes (EE-zf, EE-zm, UR-zg) have a much higher conductivity than the clay and peat classes. Since the deposits of these sand classes are embedded in low conductivity layers, they are part of the aquitard and modeled as such.

Table 3 shows the variogram models for the litho-layers as derived from the borehole data. The range of the variogram model of litho-class UR-zg could not be estimated, and is set to an arbitrary value of 400 m. The interpolation is performed using block kriging at a grid with 250 m wide cells and a block discretization of sixteen points. A minimum of four and a maximum of sixteen observations is used for each interpolation.

HESSD
12, 4191–4231, 2015

4 Results

4.1 Maximum likelihood results using calibrated resistance

The calibrated vertical resistance from the groundwater model is divided over the seven litho-classes, according to the method described in Sect. 2. The result is shown in Fig. 5. The major part of the vertical resistance is assigned to the EE-k and EE-kz litho-classes. As expected, the contributions of the litho-classes of coarser deposits to the total vertical resistance of the aquitard is small. The resistance assigned to these classes by the ML method appears to be low, compared to the clay deposits. Beside the high conductivity of the sediments, these sandy litho-classes exist only in a minority of the observations. This leads to thin litho-layers in the majority of the study area (Fig. 6), and thus a negligible contribution to the vertical resistance. Hereafter, we focus on the two most important litho-classes EE-k (clay) and EE-kz (sandy clay).

Figure 7 shows the ML thickness of litho-classes EE-k and EE-kz compared to the mean values of the PDFs of the interpolation. As can be seen, the ML method is able to reduce the litho-layer thickness to negligible values in the area where the aquitard is absent, whereas kriging interpolation results in more smooth patterns. The steep gradient of the layer thickness is more in agreement with the C values in the groundwater model as well as the geological understanding.

The ML method yields for each litho-class for each grid cell the most likely resistance, thickness and conductivity values. The position of these ML values in their prior probability distribution can be indicated by the corresponding cumulative probability value. These cumulative probabilities of the litho-layer thickness, the vertical resistance, and the hydraulic conductivity of litho-class EE-k are depicted in Fig. 8. The same data for litho-class EE-kz are depicted in Fig. 9. The data of these pictures are generated using the aquitard resistance before and after calibration of the groundwater model.

The uncertainties of the observations of the litho-layer thickness and the vertical conductance are all represented by PDFs. In Fig. 8, for litho-class EE-k, and in Fig. 9, for litho-class EE-kz, it can be seen that the cumulative probabilities of the litho-layer

HESSD
12, 4191–4231, 2015

thickness are mainly less than 0.5, which denotes the median of the PDF, for both the uncalibrated and the calibrated case. The maps of the vertical conductivities give a different picture. For litho-class EE-k, the majority of the values of the uncalibrated case are above 0.5, whereas the majority of the values for the calibrated case are below 0.5. The picture of the uncalibrated case of litho-class EE-kz is less pronounced, only the lower right corner shows some high values. However, in the calibrated case the majority of the values is far below 0.5. So calibration reduces the conductivity and increases the thickness of the litho-layers, compared to the uncalibrated case. The distribution of the vertical conductivity is described in more detail in Sect. 4.2.

4.2 Distribution of posterior conductivities

The prior distributions of the litho-class conductivities, i.e. the distributions obtained from the REGIS system, represent the best estimates given the available hydrogeological knowledge. One goal of the ML method is to improve these distributions. The CDFs of the conductivity values of litho-class EE-k and EE-kz, as discussed in the former section, are shown in Fig. 10. Herein, the prior conductivity distribution of the REGIS system and the conductivity distributions based on the uncalibrated and the calibrated C values are depicted. In fact, these distributions are spatial frequency distributions of the ML values. Nevertheless, when applied to unobserved locations, these functions can act as a probability distribution. Hereafter, the distributions will be denoted by CDF or PDF.

In the study area, the majority of the calibrated C values is higher than the uncalibrated values. Consequently, the corresponding conductivity values must be lower or the layer thickness must be higher for the calibrated situation compared to the uncalibrated one. From Fig. 10 it is clear that the conductivities from the calibrated case are much lower than the conductivities of the uncalibrated case. Only conductivity values with a corresponding ML layer thickness greater than 0.05 m are used to create these CDFs. The presented conductivity distributions are derived at the scale of the used

HESSD
12, 4191–4231, 2015

groundwater model. Since no full downscaling to core scale is applied, these CDFs are valid at this model scale and can not be used as core scale distributions.

The results are based on a small study area and can currently not be extrapolated to the whole REGIS database.

4.3 Sensitivity to prior layer thickness uncertainty

The observed litho-layer thicknesses of the available borehole data are expected to be uncertain, but the variance and distribution type are unknown. However, the proposed method needs probability distributions of these observations. As stated in Sect. 2.4, we tested the effect of several prior distributions to describe this thickness. The types of probability distributions tested are the normal and log-normal distribution. Both distributions are tested with different values of the variance. The mean value of each distribution is set to the observed thickness.

For a given litho-layer the observations of the layer thickness fall into two groups: one with the observed litho-classes and one group with the litho-classes observed absent. These groups are denoted as observed-thickness and zero-thickness, respectively. Two characteristics of the PDFs are important when judging the usability, the probability of negative values and the width of the distribution. We defined the latter as the width of the 95 % probability interval, which is the distance between the 2.5 and the 97.5 % quantiles. In Table 4, an example is shown of the effect of the standard deviation assigned to the group of observed-thicknesses. The mean value presented is a round-off value as defined in Table 1. When applied to the litho-layers, the observed litho-layer thicknesses are used as mean value for the PDFs. Table 5 shows the same information for the zero-thickness observations.

Interpolation of the litho-layer thicknesses are performed using the settings as described above. The normal distribution often yields negative ML thicknesses (column percentile < 0) which makes this distribution unusable. Therefore, the log-normal distribution is used to describe the litho-layer uncertainty. In Fig. 11, the effect of the different variance settings on the interpolation of litho-class EE-kz, using log-normal distribu-

HESSD
12, 4191–4231, 2015

tions, is shown. In this figure, the maps in each row are calculated using the same zero-thickness variance. The maps in each column are calculated using the same observed-thickness variance. The maps with high variance of observed-thickness (right column) show unlikely high variances at the area where this litho-class is present. Therefore, this variance setting is rejected. The difference between the low variance (left column) and the medium variance maps (middle column) is not very pronounced. The major difference is the sensitivity to observations with a high variance. In the center of the medium variance map (middle column), one observation location yields a very high variance. In one borehole, the litho-layer of litho-class EE-kz is here described with forty-nine sub-layers of one meter each with each their own variance. After summation, this yields a very high variance for this location. For further processing the medium variance is used.

The lower-left and the upper-right corner of the study area are dominated by zero-thickness observations. The variances shown in these areas of the low (upper row) and medium variance (middle row) are low compared to areas dominated by the observed-thickness locations. Therefore, the high variance settings (lower row) for the zero-thickness observations are used for further ML analysis. Corollary, for further calculations the medium variance for the observed-thickness locations is used and the high variance for the zero-thickness locations.

4.4 Evaluation of kriging options

Depending on the nature of the observed data, and the associated assumptions of the underlying random field model, the appropriate form of data-transformation and kriging is chosen before performing kriging interpolation. Herewith, a decision has to be made whether or not to perform a data transformation. Hereafter, the decisions made are justified.

Layer thicknesses are, obviously, required to be greater than or equal to zero. Therefore, not every PDF is appropriate to describe the uncertain thickness. In the kriging interpolation with uncertain observations, two parameters need to be assigned a prob-

HESSD
12, 4191–4231, 2015

ability density function: the observations of the layer thickness (former section), and the interpolation error. Usually, the interpolation error is assumed to be normal distributed. No accurate information is available about the true shape of these PDFs. Therefore, the performance of the use of normal and log-normal distributions was tested. Both distributions have their own deficiency, especially when the standard deviation is large compared to the mean value. In that case, the normal distributions may yield negative thicknesses with too high probability, and the log-normal distribution may become very skewed. The latter is a disadvantage in finding representative ML values because of the difference between the mode and the mean of the distribution. Because of the potential negative values of the normal distribution, the log-normal distribution is tested for the interpolation error as well.

One way to avoid negative interpolated values is to transform the observations to their log values before interpolation, and back-transform them afterwards. Applied to block-kriging, the different way the block average is calculated has to be considered. When kriging the log-transformed values, the block average is the geometric mean, kriging the non-transformed values yields the arithmetic mean. In Fig. 12, a comparison is made between interpolation of the thickness PDFs and the log-transformed thickness PDFs. With both methods, the interpolated thicknesses close to the observations are quite in agreement with the observed values. However, at larger distance the difference between the two methods is larger, with interpolated thicknesses from the log-transformed kriging being very low. From geological point of view this is not a feasible result. Even when the ranges of the variograms are increased, three times larger than derived from the data, the interpolated thickness remains much lower than presumed, given the observations. Thus the non-log-transformed kriging variant provides a better option.

HESSD
12, 4191–4231, 2015

5 Discussion and conclusions

The implementation of the maximum likelihood (ML) method, in conjunction with kriging interpolation, appears useful in updating hydrogeological information from borehole data, with information derived from calibrated groundwater models. From the uncertain hydrogeological data, described by a multidimensional probability density function, the most likely parameter values are derived given the information available from calibrated parameter values in groundwater models. The ML method is applied to layer thicknesses and vertical conductivities at litho-class support. Herewith, the most likely litho-layer thickness and vertical conductivity values are obtained for the studied aquitard.

In the REGIS database the a priori probability distributions of the vertical conductivity, for a given litho-class, are assumed location independent. The posterior distributions of the two most important litho-classes show much less variability than the corresponding prior distributions do. This can be expected as additional knowledge is added using results from a calibrated groundwater model. However, at this point this is yet not a reason to update the prior distribution in the REGIS database, because the posterior distribution is based on a small study area, while the prior distribution is based on data from the whole data base. Moreover, it is not unlikely that the a priori distribution of the vertical conductivity of a litho-class is spatially varying. Subsequent application of this method to a larger area will give more certainty about this.

The values of some parameters, obtained by the ML method, show a strong systematic deviation from the prior distribution, with the majority of the values either lower or higher than the median of the prior distribution. In case of a data update the posterior distribution should of course divert from the prior distribution, but a strong systematic deviation may indicate errors, either caused by data errors or a wrong perception about the hydrological system. The proposed method can thus serve as a tool to guide the discussion between experts from different domains.

With the described method, the ML values of the PDFs are derived for each layer separately, neglecting the thickness of adjacent layers. Obviously, it is not possible to

HESSD
12, 4191–4231, 2015

change the thickness of a layer without affecting the thickness of the adjacent layers. The present study does not take this into account and only aims to describe a method to find the most likely combination of layer thickness and conductivity. A future study should account for all layers of the hydrogeological model, where the sum of all model-layer thicknesses is constrained and, preferably, described by RVs.

The proposed method assigns a PDF to the thickness of every single litho-layer from the borehole descriptions. In Sect. 4.3 an example is shown where this yields an unlikely high variance for a thickness observation. When adjacent litho-layers are of the same litho-class, aggregation of these litho-layers before assigning a variance may give a more appropriate representation of the uncertainty. This may yield a more realistic uncertainty description of the thickness observations.

As with the assignment of litho-classes, also the calibrated vertical resistance of the groundwater model is regarded as perfectly known. A valuable extension to the presented method is to account for uncertainty of the calibration results.

The use of piecewise linear PDFs, instead of parametrized PDFs, makes it possible to perform the necessary calculations without the burden of deriving intractable analytical solutions or resort to time-consuming Monte Carlo analysis. Herewith, many different calculations can be tested with relatively little effort.

Appendix A: Likelihood of elementary operations

This section contains the derivations of calculating the maximum likelihood (ML) of the result of an elementary operation. All random variables (RV) are described by piecewise linear probability density functions (PDF).

Hereafter, X and Y are known independent RVs and Z is the resulting RV of an elementary operation. For every value $x \in X$ and $y \in Y$ the probability density of the joint distribution can be calculated as

$$p(x,y) = f_{x_i}(x) f_{y_j}(y), \tag{A1}$$

HESSD
12, 4191–4231, 2015

where $f_x(x)$ and $f_y(y)$ are the PDFs of X and Y, respectively. The subscripts i and j denote the bin numbers of the piecewise linear PDFs. The PDFs are defined as

$$f_{x_i}(x) = p_{0,x_i} + r_{x_i} x \tag{A2}$$

$$f_{y_j}(y) = p_{0,y_j} + r_{y_j} y, \tag{A3}$$

where p_{0,x_i} and p_{0,y_j} are the probability densities at $x = 0$ for bin i and $y = 0$ for bin j, respectively, and r_{x_i} and r_{y_j} are constant values.

Applying elementary operations, x can be written as a function of z and y as

$$x = g(y, z). \tag{A4}$$

Inserting Eqs. (A2)–(A4) into Eq. (A1) yields

$$p(y, z) = (p_{0,x_i} + r_{x_i} g(y, z))(p_{0,y_j} + r_{y_j} y). \tag{A5}$$

The extreme values of $p(g(y, z), y)$ for a certain value of z can be found by taking the first derivative with respect to y, which writes

$$\frac{\mathrm{d}p(y, z)}{\mathrm{d}y} = p_{0,x_i} r_{y_j} + r_{x_i} p_{0,y_j} \frac{\mathrm{d}g(y, z)}{\mathrm{d}y} + r_{x_i} r_{y_j} \frac{\mathrm{d}g(y, z)y}{\mathrm{d}y}. \tag{A6}$$

Setting this function equal to 0 and solve it for y yields the coordinates (x, y) with an extreme value for $p(x, y)$. Since this function only holds within the domain of the joint bin (i, j), the value of y must satisfy the constraint $y \in [y_j, y_{j+1}]$, where y_j and y_{j+1} are the boundaries of the bin j of Y.

In the next sections this method is applied to four elementary operations.

HESSD
12, 4191–4231, 2015

A1 Summation

Let $Z = X + Y$, thus $g(y,z) = z - y$. The first derivative with respect to y of Eq. (A6) yields:

$$\frac{\mathrm{d}p(y,z)}{\mathrm{d}y} = p_{0,x_i} r_{y_j} + r_{x_i} p_{0,y_j} \frac{\mathrm{d}(z-y)}{\mathrm{d}y} \tag{A7}$$
$$= p_{0,x_i} r_{y_j} - r_{x_i} p_{0,y_j} + r_{x_i} r_{y_j} z - 2 r_{x_i} r_{y_j} y.$$

Setting this function to 0 and solve it for y yields

$$y = (p_{0,x_i} r_{y_j} - r_{x_i} p_{0,y_j} + r_{x_i} r_{y_j} z)/(2 r_{x_i} r_{y_j}). \tag{A8}$$

A2 Subtraction

Let $Z = X - Y$, thus $g(y,z) = z + y$. The first derivative with respect to y of Eq. (A6) yields

$$\frac{\mathrm{d}p(y,z)}{\mathrm{d}y} = p_{0,x_i} r_{y_j} + r_{x_i} p_{0,y_j} \frac{\mathrm{d}(z+y)}{\mathrm{d}y} + r_{x_i} r_{y_j} \frac{\mathrm{d}(z+y)y}{\mathrm{d}y} \tag{A9}$$
$$= p_{0,x_i} r_{y_j} + r_{x_i} p_{0,y_j} + r_{x_i} r_{y_j} z + 2 r_{x_i} r_{y_j} y.$$

Setting this function to 0 and solve it for y yields

$$y = (p_{0,x_i} r_{y_j} + r_{x_i} p_{0,y_j} + r_{x_i} r_{y_j} z)/(-2 r_{x_i} r_{y_j}). \tag{A10}$$

A3 Multiplication

Let $Z = XY$, thus $g(y,z) = z/y$. The first derivative with respect to y of Eq. (A6) yields

$$\frac{\mathrm{d}p(y,z)}{\mathrm{d}y} = p_{0,x_i} r_{y_j} + r_{x_i} p_{0,y_j} \frac{\mathrm{d}(z/y)}{\mathrm{d}y} + r_{x_i} r_{y_j} \frac{\mathrm{d}(z/y)y}{\mathrm{d}y} \tag{A11}$$
$$= p_{0,x_i} r_{y_j} - r_{x_i} p_{0,y_j} z y^{-2}.$$

HESSD
12, 4191–4231, 2015

Setting this function to 0 and solve it for y yields

$$y = \pm\sqrt{\frac{r_{x_i} p_{0,y_j} z}{p_{0,x_i} r_{y_j}}}. \tag{A12}$$

A4 Division

Let $Z = X/Y$, thus $g(y,z) = zy$. The first derivative with respect to y of Eq. (A6) yields

$$\begin{aligned}\frac{\mathrm{d}p(y,z)}{\mathrm{d}y} &= p_{0,x_i} r_{y_j} + r_{x_i} p_{0,y_j} \frac{\mathrm{d}(zy)}{\mathrm{d}y} + r_{x_i} r_{y_j} \frac{\mathrm{d}(zy)y}{\mathrm{d}y} \\ &= p_{0,x_i} r_{y_j} + r_{x_i} p_{0,y_j} z + 2 r_{x_i} r_{y_j} zy.\end{aligned} \tag{A13}$$

Setting this function to 0 and solve it for y yields

$$y = (p_{0,x_i} r_{y_j} + r_{x_i} p_{0,y_j} z)/(-2 r_{x_i} r_{y_j} z). \tag{A14}$$

References

Carrera, J., Alcolea, A., Medina, A., Hidalgo, J., and Slooten, L. J.: Inverse problem in hydrogeology, Hydrogeol. J., 13, 206–222, doi:10.1007/s10040-004-0404-7, 2005. 4193

Dagan, G.: Statistical theory of groundwater flow and transport: pore to laboratory, laboratory to formation, and formation to regional scale, Water Resour. Res., 22, 120–134, doi:10.1029/WR022i09Sp0120S, 1986. 4193

de Lange, W. and Borren, W.: Grondwatermodel AZURE versie 1.0, Tech. rep., Deltares, the Netherlands, 2014. 4193, 4196, 4202

Deutsch, C. V.: Correcting for negative weights in ordinary kriging, Comput. Geosci., 22, 765–773, doi:10.1016/0098-3004(96)00005-2, 1996. 4199

Fiori, A., Dagan, G., and Jankovic, I.: Upscaling of steady flow in three-dimensional highly heterogeneous formations, Multiscale Model. Sim., 9, 1162–1180, doi:10.1137/110820294, 2011. 4193

HESSD
12, 4191–4231, 2015

Goovaerts, P.: Geostatistics For Natural Resources Evaluation, Oxford University Press, New York, NY, USA, 1997. 4199
Hendricks Franssen, H., Alcolea, A., Riva, M., Bakr, M., van der Wiel, N., Stauffer, F., and Guadagnini, A.: A comparison of seven methods for the inverse modelling of groundwater flow, application to the characterisation of well catchments, Adv. Water Resour., 32, 851–872, doi:10.1016/j.advwatres.2009.02.011, 2009. 4193
Hoteit, I., Luo, X., and Pham, D.-T.: Particle kalman filtering: a nonlinear bayesian framework for ensemble kalman filters, Mon. Weather Rev., 140, 528–542, doi:10.1175/2011MWR3640.1, 2012. 4193
Isaaks, E. H. and Srivastava, R. M.: An Introduction to Applied Geostatistics, Oxford University Press, New York, NY, USA, 1989. 4198
Kaczynski, W., Leemis, L., Loehr, N., and McQueston, J.: Nonparametric random variate generation using a piecewise-linear cumulative distribution function, Commun. Stat. Simul. Comput., 41, 449–468, doi:10.1080/03610918.2011.606947, 2012. 4195
Mood, A. M., Graybill, F. A., and Boes, D. C.: Introduction to the Theory of Statistics, 3rd edn., McGraw-Hill Higher Education, Singapore, 1974. 4196
Nilsson, B., Højberg, A. L., Refsgaard, J. C., and Troldborg, L.: Uncertainty in geological and hydrogeological data, Hydrol. Earth Syst. Sci., 11, 1551–1561, doi:10.5194/hess-11-1551-2007, 2007. 4192
Nœtinger, B., Artus, V., and Zargar, G.: The future of stochastic and upscaling methods in hydrogeology, Hydrogeol. J., 13, 184–201, doi:10.1007/s10040-004-0427-0, 2005. 4193
Rogiers, B., Vienken, T., Gedeon, M., Batelaan, O., Mallants, D., Huysmans, M., and Dassargues, A.: Multi-scale aquifer characterization and groundwater flow model parameterization using direct push technologies, Environ. Earth Sci., 72, 1303–1324, doi:10.1007/s12665-014-3416-1, 2014. 4192
Sanchez-Vila, X., Guadagnini, A., and Carrera, J.: Representative hydraulic conductivities in saturated groundwater flow, Rev. Geophys., 44, 1–46, doi:10.1029/2005RG000169, 2006. 4193
Tolosana-Delgado, R. and Pawlowsky-Glahn, V.: Kriging regionalized positive variables revisited: sample space and scale considerations, Math. Geol., 39, 529–558, doi:10.1007/s11004-007-9107-7, 2007. 4198

HESSD
12, 4191–4231, 2015

Valstar, J. R., McLaughlin, D. B., te Stroet, C. B. M., and van Geer, F. C.: A representer-based inverse method for groundwater flow and transport applications, Water Resour. Res., 40, W05116, doi:10.1029/2003WR002922, 2004. 4193

Vander Wielen, M. J. and Vander Wielen, R. J.: The general segmented distribution, Commun. Stat. Theory, doi:10.1080/03610926.2012.758743, in press, 2015. 4195

Vernes, R. W. and van Doorn, T.: REGIS II, a 3D hydrogeological model of the Netherlands, in: Proceedings of the Philadelphia Philadelphia, PA, USA, 22 October 2006, 22-25 October 2006, 39-12, 2006 GSA Annual Meeting, The Geological Society of America, Geological Society of America, Abstracts with Programs, 38, p. 109, 2006. 4193, 4195

Vernes, R., van Doorn, T., Bierkens, M., van Gessel, S., and de Heer, E.: Van Gidslaag naar Hydrogeologisch Eenheid, Toelichting op de totstandkoming van de dataset REGIS II (in Dutch), Tech. rep., Nederlands Instituut voor Toegepaste Geowetenschappen TNO – Geological Survey of the Netherlands, Utrecht, the Netherlands, available at: http://www2.dinoloket.nl/data/download/maps/resources/Rapport_NITG_05-038-B0115_netversie.pdf (last access: 21 April 2015), 2005. 4193, 4195

Zimmerman, D. A., de Marsily, G., Gotway, C. A., Marietta, M. G., Axness, C. L., Beauheim, R. L., Bras, R. L., Carrera, J., Dagan, G., Davies, P. B., Gallegos, D. P., Galli, A., Gómez-Hernández, J., Grindrod, P., Gutjahr, A. L., Kitanidis, P. K., Lavenue, A. M., McLaughlin, D., Neuman, S. P., RamaRao, B. S., Ravenne, C., and Rubin, Y.: A comparison of seven geostatistically based inverse approaches to estimate transmissivities for modeling advective transport by groundwater flow, Water Resour. Res., 34, 1373–1413, doi:10.1029/98WR00003, 1998. 4193

HESSD
12, 4191–4231, 2015

Table 1. Three classes of standard deviation related to the truncation classes.

truncation class [m]	low [m]	medium [m]	high [m]
0.01	0.002	0.01	0.05
0.05	0.010	0.05	0.25
0.10	0.020	0.10	0.50
0.50	0.100	0.50	2.50
1.00	0.200	1.00	5.00

HESSD
12, 4191–4231, 2015

Table 2. Probability data of the vertical hydraulic conductivity values of each litho-class. The distributions are defined by the 2.5 and 97.5 % percentile values and are assumed to be log-normal. The presented mean and SD are derived from the PDFs.

litho-class	2.5 % [$m\,d^{-1}$]	97.5 % [$m\,d^{-1}$]	mean [$m\,d^{-1}$]	sd [$m\,d^{-1}$]	description
EE-k	7.3×10^{-5}	0.0219	3.64×10^{-3}	9.74×10^{-3}	Eem Formation, clay
EE-kz	7.3×10^{-5}	0.301	4.46×10^{-2}	0.372	Eem Formation, sandy clay
EE-v	6.4×10^{-4}	0.32	5.03×10^{-2}	0.166	Eem Formation, peat
EE-zf	7.3×10^{-5}	2.88	0.548	12.4	Eem Formation, fine sand
EE-zm	1.4	29.7	8.74	7.98	Eem Formation, medium sand
UR-kz	1.7×10^{-4}	0.29	4.25×10^{-2}	0.239	Urk Formation, sandy clay
UR-zg	2.4	160.7	34.9	51.2	Urk Formation, coarse sand

HESSD
12, 4191–4231, 2015

Table 3. Variogram model for thickness of each litho-class.

litho-class	type	range [m]	sill [m^2]
EE-k	exponential	1800	43
EE-kz	exponential	2000	42
EE-v	exponential	4000	0.5
EE-zf	exponential	1200	6
EE-zm	exponential	800	6
UR-kz	exponential	300	5
UR-zg	exponential	–	4

HESSD
12, 4191–4231, 2015

Table 4. Effect of SD of the observed-thicknesses distributions. The mean value of 1 m, which is the round-off value, is used as an example. Other round-off values show a proportional effect.

SD	distribution	mean [m]	s.d. [m]	percentile < 0 m	thk 2.5 % [m]	thk 97.5 % [m]	95 % width [m]
low	normal	1.00	0.20	0 %	0.608	1.39	0.784
medium	normal	1.00	1.00	15.9 %	−0.961	2.96	3.92
high	normal	1.00	5.00	42.1 %	−8.80	10.8	19.6
low	log-normal	1.00	0.20	0 %	0.665	1.45	0.781
medium	log-normal	1.00	1.00	0 %	0.138	3.62	3.48
high	log-normal	1.00	5.00	0 %	0.0057	6.76	6.75

HESSD
12, 4191–4231, 2015

Table 5. Effect of the SD of the zero-thickness distributions.

SD	distribution	mean [m]	s.d. [m]	percentile < 0 m	thk 2.5 % [m]	thk 97.5 % [m]	95 % width [m]
low	normal	0.005	0.10	48.0 %	−0.190	0.201	0.392
medium	normal	0.050	1.00	48.0 %	−1.91	2.01	3.92
high	normal	0.100	2.00	48.0 %	−3.82	4.02	7.84
low	log-normal	0.005	0.10	0 %	2.1×10^{-6}	0.0304	0.0304
medium	log-normal	0.050	1.00	0 %	2.1×10^{-5}	0.304	0.304
high	log-normal	0.100	2.00	0 %	4.1×10^{-5}	0.608	0.608

HESSD
12, 4191–4231, 2015

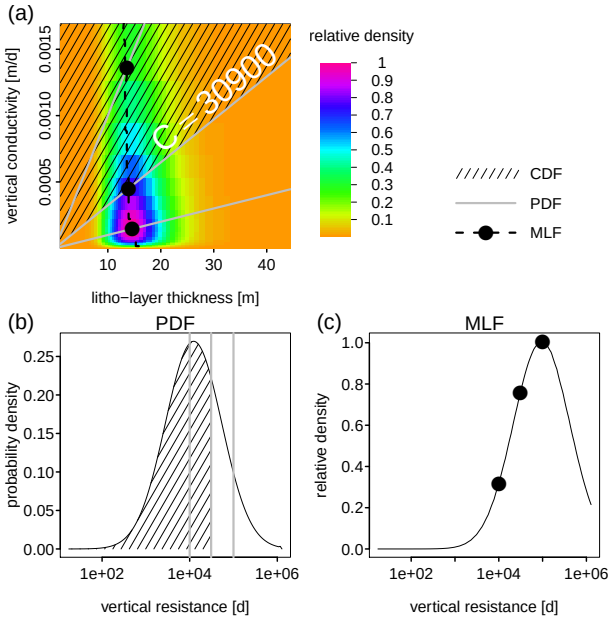

Figure 1. Connection of **(a)** the joint PDF of the litho-layer thickness and conductivity with **(b)** the PDF, and **(c)** the MLF of the *C* value. The gray lines denote equi *C*-lines.

HESSD
12, 4191–4231, 2015

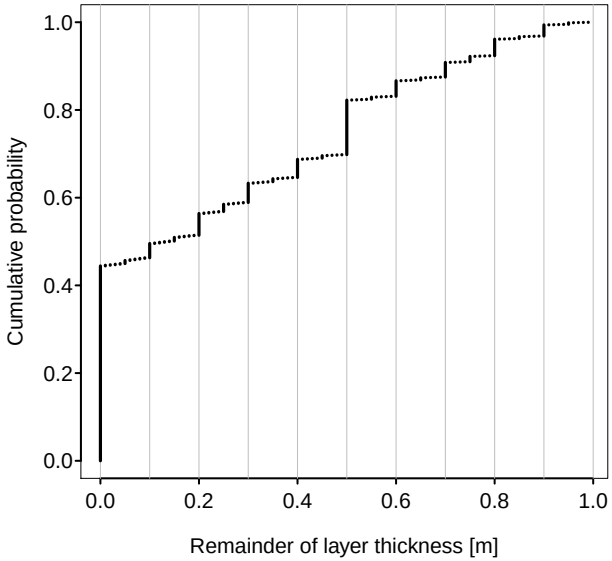

Figure 2. Cumulative distribution of the remainder of about 475 000 litho-layer thicknesses after division by one meter. The vertical lines show the position of the round-off values at every ten centimeters.

HESSD
12, 4191–4231, 2015

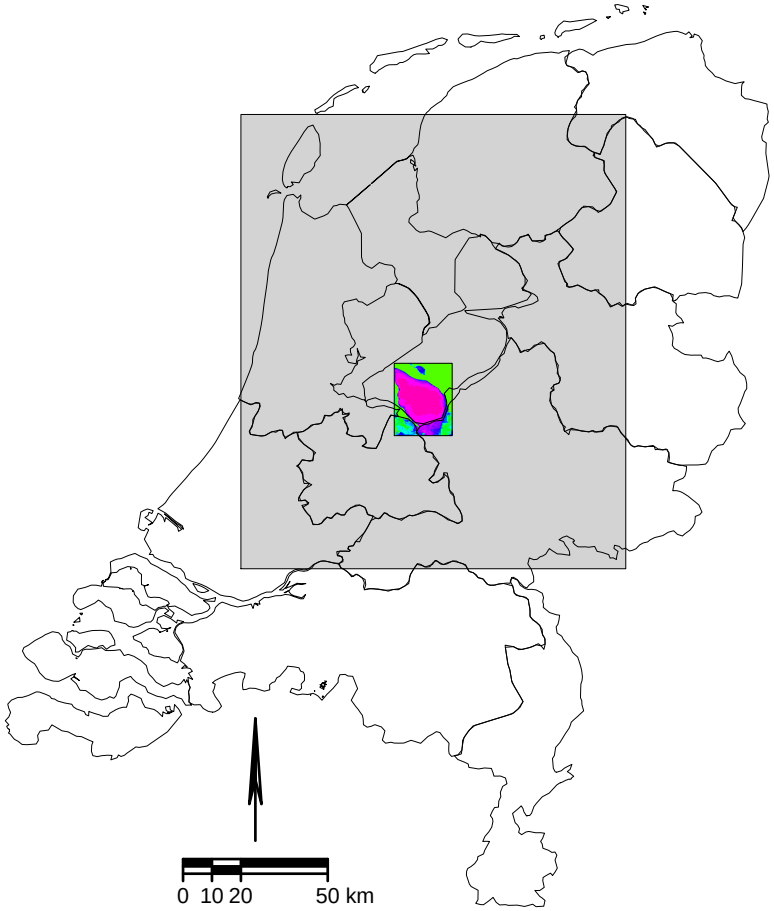

Figure 3. Study area. The gray area is the extent of the Azure groundwater model. The small rectangle denotes the study area with the vertical resistance, as shown in Fig. 4, depicted.

HESSD
12, 4191–4231, 2015

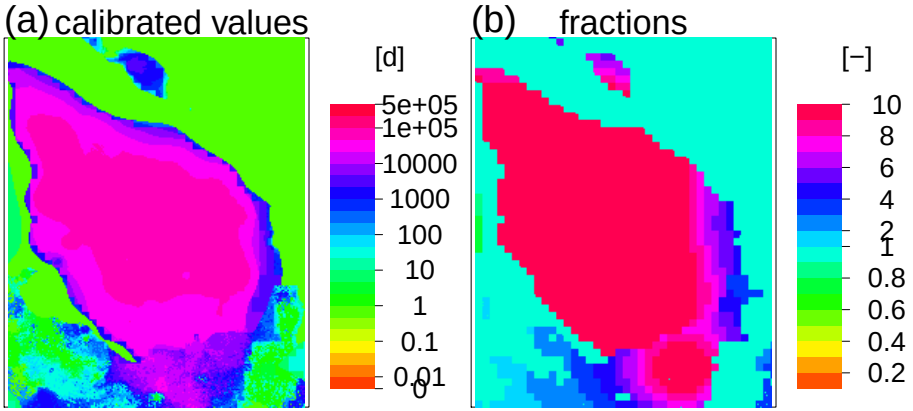

Figure 4. The **(a)** calibrated hydraulic vertical resistance of the aquitard and **(b)** the quotient of the calibrated and the uncalibrated resistance. The majority of the calibrated resistance in the clay patch is about ten times the uncalibrated resistance.

HESSD
12, 4191–4231, 2015

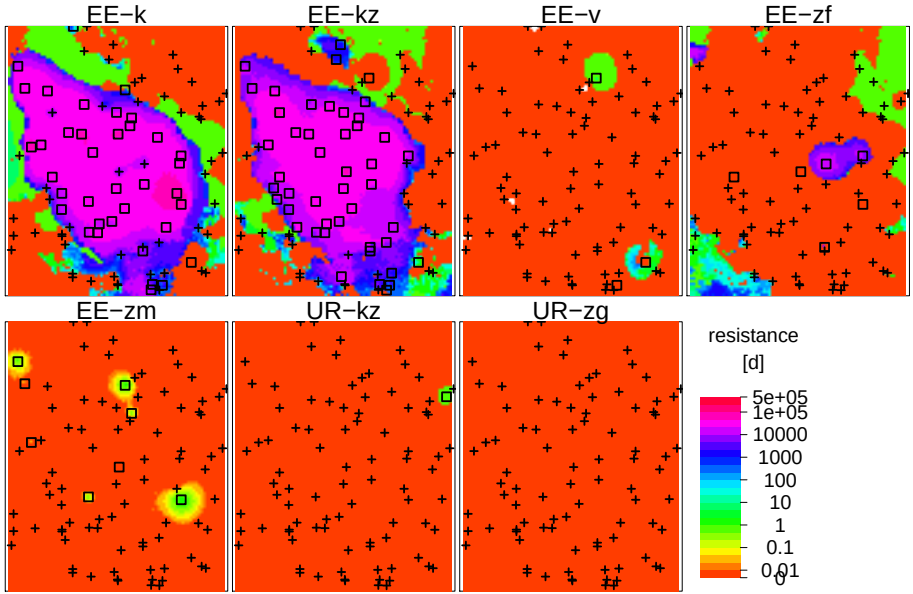

Figure 5. Most likely vertical resistance. The squares denote observations where the litho-class is present, the plus signs where it is absent.

HESSD
12, 4191–4231, 2015

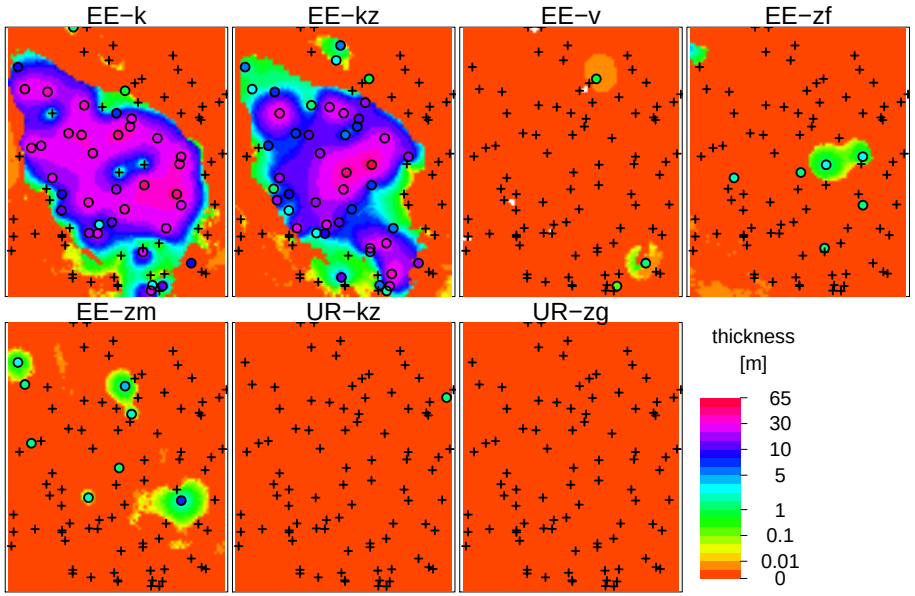

Figure 6. Most likely thickness of each litho-class. The circles denote observations where the litho-class is present, the plus signs where it is absent. The circles are colored with the observed thickness.

HESSD
12, 4191–4231, 2015

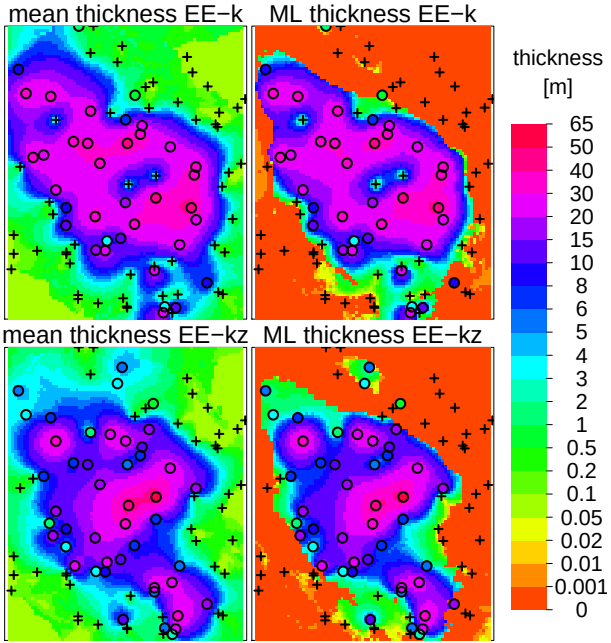

Figure 7. Thickness of litho-class EE-k (top) and EE-kz (bottom). Mean kriging thickness (left) compared to ML thickness (right).

HESSD
12, 4191–4231, 2015

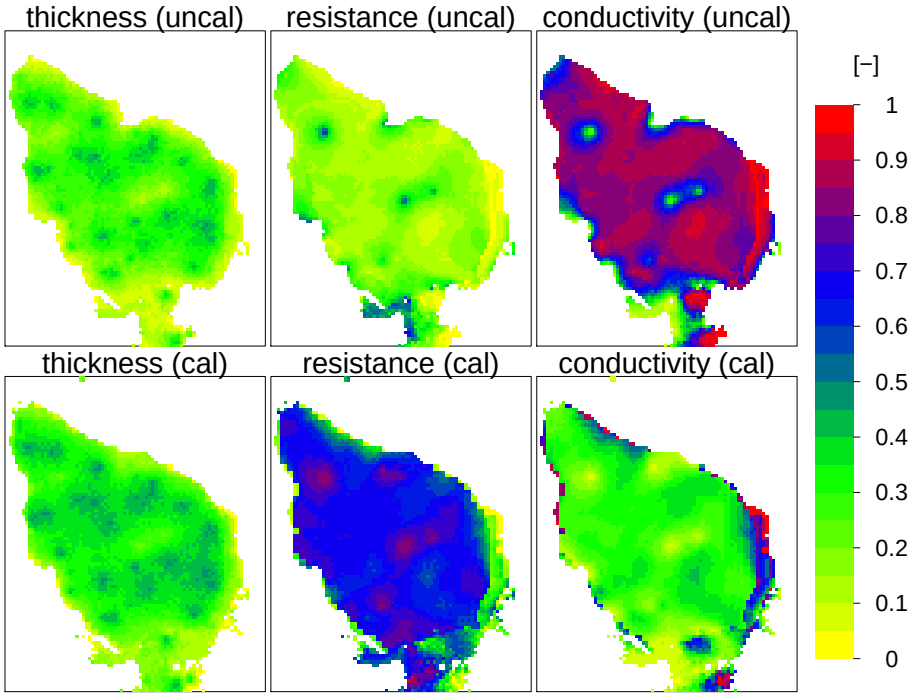

Figure 8. Cumulative probability of the ML values of the uncalibrated (top) and calibrated (bottom) parameters of litho-class EE-k. The data is clipped at 0.05 m of the ML thickness.

HESSD
12, 4191–4231, 2015

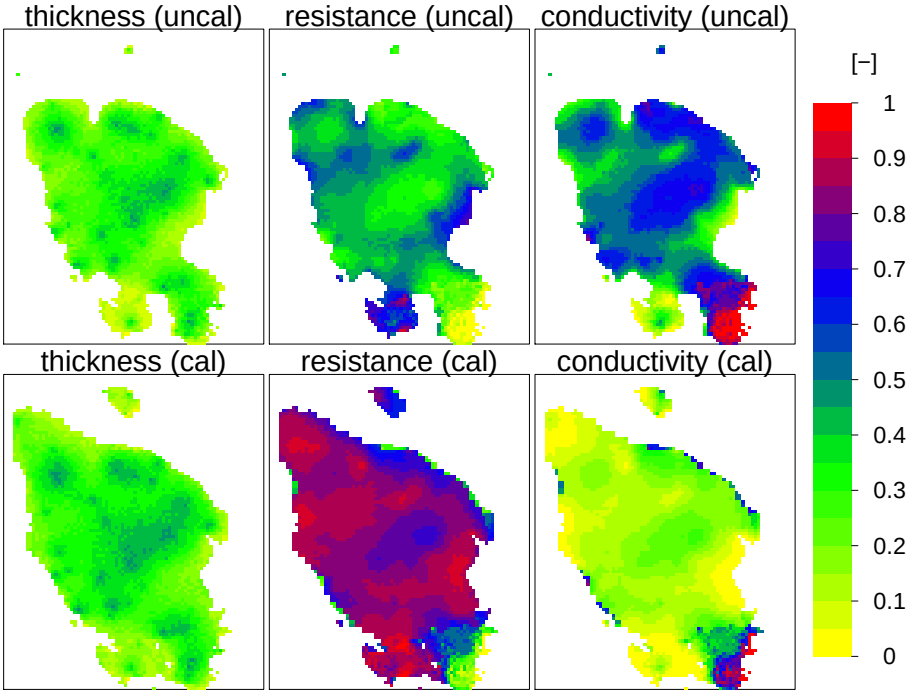

Figure 9. Cumulative probability of the ML values of the uncalibrated (top) and calibrated (bottom) parameters of litho-class EE-kz. The data is clipped at 0.05 m of the ML thickness.

HESSD
12, 4191–4231, 2015

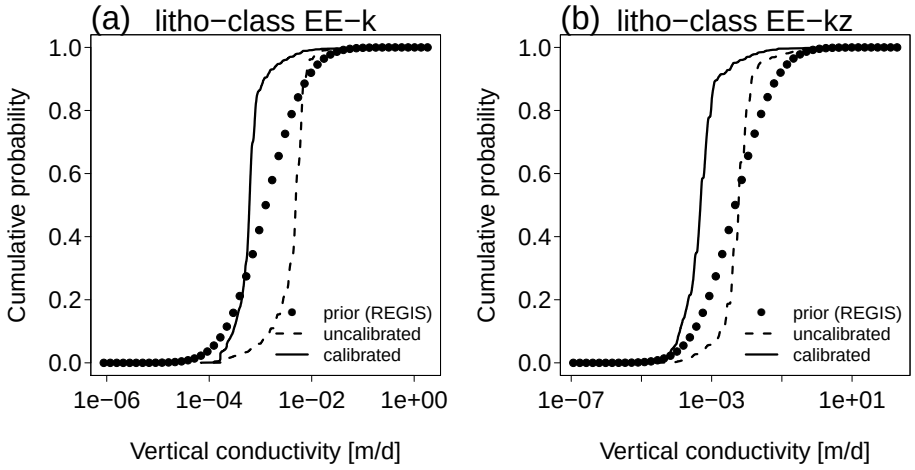

Figure 10. Comparison of conductivity distributions of litho-class **(a)** EE-k and **(b)** EE-kz. Shown are the prior distribution of the REGIS system (dots), the distribution based on the uncalibrated *C* values (dashed line), and the distribution based on the calibrated *C* values (solid line). The *x* axis is at log-scale.

HESSD
12, 4191–4231, 2015

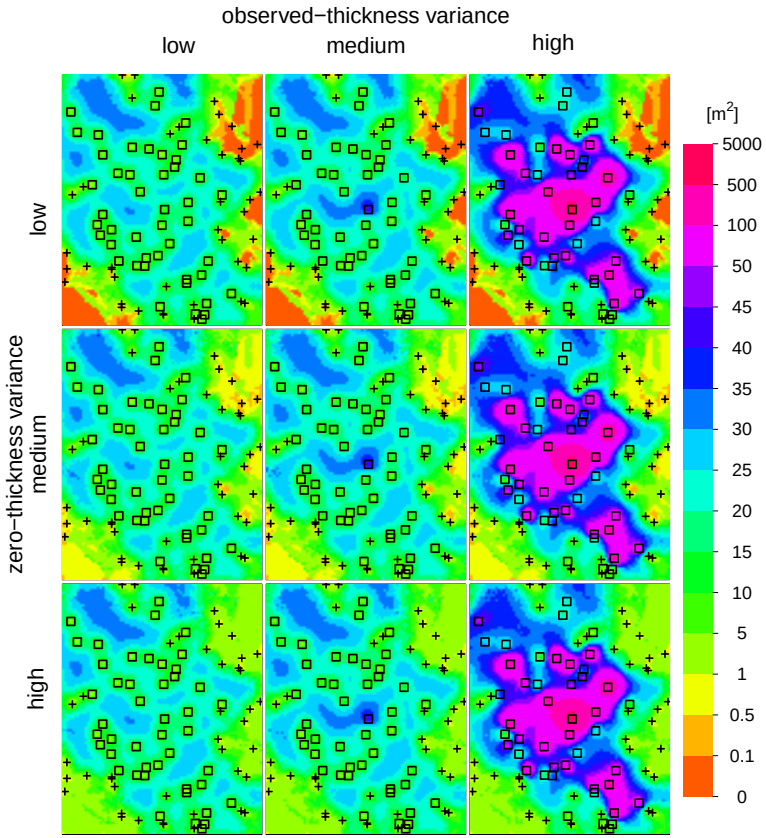

Figure 11. Maps of interpolation variances of litho-class EE-kz for different settings of the observation variances. The used settings for the variances are shown in Tables 4 and 5. The squares denote the observed-thickness locations and the plus signs the zero-thickness locations.

HESSD
12, 4191–4231, 2015

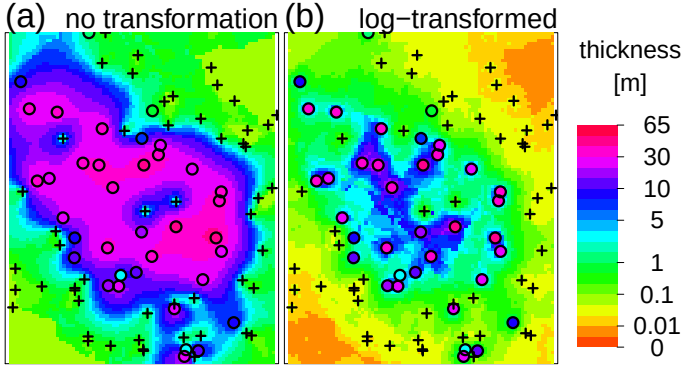

Figure 12. Mean value of interpolated layer thickness of litho-class EE-k. Shown is **(a)** kriging without data transformation, and **(b)** kriging with log-transformed data. The circles denote observations with the litho-class present, the plus signs where it is absent. The circles are colored with the observed thickness.

HESSD
12, 4191–4231, 2015